ELSEVIER

Journal of Alloys and Compounds 235 (1996) 112–119

Journal of ALLOYS AND COMPOUNDS

Co corner of the system Sm–Co–Zr: decomposition of the phase 1:7 and equilibria at 850°C

S. Derkaoui[a], N. Valignat[b], C.H. Allibert[b,*]

[a] *Département de Physique, Faculté des Sciences B.P. 28/S, Université Ibnou Zohr, 8000 Agadir, Morocco*

[b] *Laboratoire de Thermodynamique et de Physico-Chimie Métallurgiques, associé au CNRS (URA 29), E.N.S.E.E.G., BP. 75, 38402 Saint Martin d'Hères, France*

Received 13 September 1995; in final form 6 October 1995

Abstract

In the Co range 100–75 at.% of the system Sm–Co–Zr, the phase equilibria at 850°C are determined by composition and crystal structure analysis of annealed alloys. Five three-phase fields centred on the phase R2:17, based on Sm_2Co_{17}, are detected. We observe the formation of ternary phases obtained by substitution of Zr for Sm in the binary compounds $Sm_{n+1}Co_{5n-1}$ ($n = 2$–4).

The genesis of the multiphase fields centred on R2:17 involves the transformation of the high-temperature phase 1:7. This transformation is studied by microstructural investigation. As predicted by the phase equilibria, the depletion 1:7 → 1:5 + R2:17(+ 5:19) proceeds by continuous precipitation. The reactions 1:7 → R2:17 + *Co* + 6:23 and 1:7 → *R*2:17 + 6:23 + 1:3 occur by discontinuous processes. The limiting step is the diffusion controlled growth. $\tilde{D}_{1:5}$ is evaluated at 30×10^{-20} m^2 s^{-1}. For the reactions 1:7 → R2:17 + (n + 1:5n − 1), a transient step of continuous precipitation of the coherent metastable phases is proposed.

Keywords: Phase equilibria; Sm–Co–Zr; Transformation mechanisms; 1:7 phase.

1. Introduction

The extensive investigations related to permanent magnets based on Sm(Co, Fe, Cu, Zr)$_{7-8}$ alloys reflect the significant role played by Zr on the constitution of such alloys. Zr additions to the alloys in the composition range Sm_2(Co, Fe, Cu)$_{17}$–Sm(Co, Fe, Cu)$_5$ were found to lead to a single phase at 1100–1200°C [1–3]. They also generate a typical cell microstructure by treatment at 800–850°C which consists of coherent layers of phases based on $SmCo_5$ and $SmCo_3$ forming a regular network in a matrix based on Sm_2Co_{17}. Numerous descriptions of features of the cell microstructure were reviewed in Ref. [4].

Few investigations [5,6] of ternary Sm–Co–Zr alloys at 1200–1150°C reveal the major effect of Zr on the constitution of the Sm–Co system. A comparison (Fig. 1) of the binary phase diagrams of Sm–Co [7] and Zr–Co [8] with the ternary section Sm–Co–Zr [6] shows that Zr drastically extends the single phase fields based on $SmCo_5$ and $Sm_{n+1}Co_{5n-1}$ ($n = 2$–4) at 1150°C. While the ternary phases with stoichiometric ratio n + 1:5n − 1 correspond to the substitution of Zr for Sm, the phase 1:7, based on $SmCo_5$, is formed by substitution of Zr for Co pairs in the Sm-rich region. In the Sm-poor field, 1:7 probably occurs by Zr substitution for Sm atoms as well as for Co pairs. At high temperature, these ternary results completely support the observations made on the alloys Sm(Co, Fe, Cu, Zr)$_{7-8}$ and lead to predict the quinary behaviour in a neighbouring composition range.

Consequently, knowledge of the constitutional evolution of ternary Sm–Co–Zr alloys with time at 850°C is expected to enable the prediction of quinary alloy behaviour for long agings at the temperature of the cell microstructure genesis and for other compositions.

Accordingly ,the purpose of the present work is to study the solid state phase equilibria of Sm–Co–Zr alloys with Co contents 100–75 at.% at 850°C and to

* Corresponding author.

SSDI 0925-8388(95)02119-1

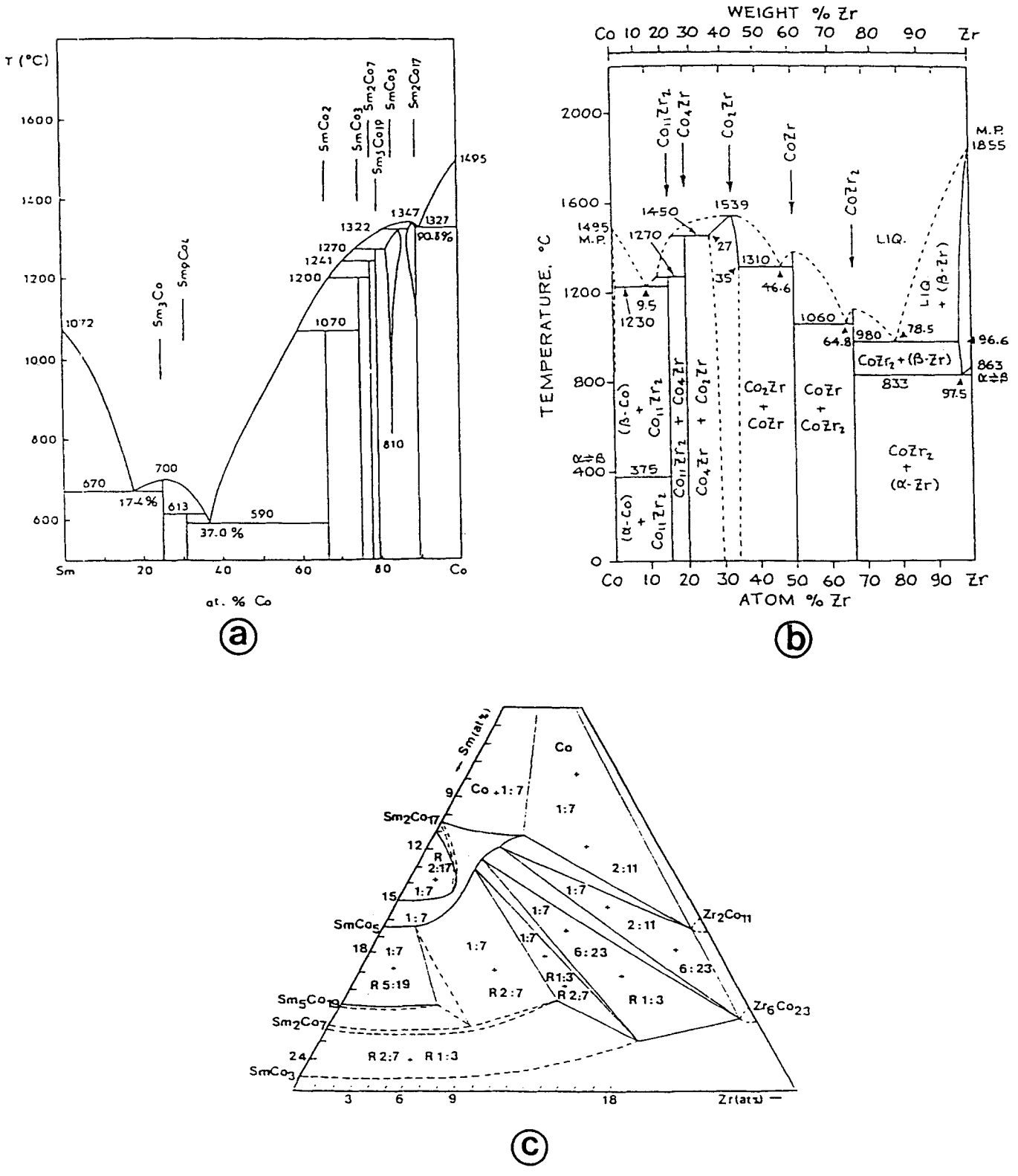

Fig. 1. Phase diagrams of the systems (a) Sm–Co [7], (b) Zr–Co [8] and (c) isothermal section Sm–Co–Zr at 1150°C [6].

identify the transformations of the supersaturated 1:7 phase by aging at this temperature.

2. Experimental

The samples were prepared by induction melting of pieces of Sm ingots (99.5%), of electrolytic Co (99.95%) and chips of Zr (99.8%). The cast alloys were submitted to two series of high temperature treatments (Q or C) prior to aging (A), carried out at 850°C, for periods from 50 to 720 h, under ultra-pure Argon. The first series (Q) involved a prehomogenization (2 h) at 10°C below the solidus temperature, then an annealing (14 h) at 1150°C, followed by quenching at 300 K min^{-1} to room temperature. The second series (C) included a complementary annealing (2 h) at 1150°C then a cooling at 2 K min^{-1} to room temperature. These treatments are referred to as Q and C to show that the initial state of the aging corresponds either to a quenched supersaturated state, or to a slowly cooled state.

The phases present in the aged samples were analysed by X-ray diffraction (XRD), microprobe analysis (EPMA) and scanning electron microscopy (SEM).

3. Results

3.1. Phase equilibria at 850°C

The phase equilibria are plotted from the compositions and structures of the phases observed in specimens submitted to two types of treatments: Q + A(850°C, 600 h) and C + A(850°C, 240 or 720 h). The conditions of these treatments were selected from numerous attempts to provide microstructures with phase sizes large enough for a reliable microprobe analysis (3–4 μm). Despite the long durations of the aging, the microstructure coarsening was weak. It was not significantly enhanced by the slow cooling rate used in C in order to promote nucleation at relatively high temperatures of the phases to be precipitated at low temperature. In most specimens, the local measurements of the phase compositions were complemented by plots of concentration profiles through two phase mixtures. This evidenced that in some specimens, the equilibrium state was not completely reached after 600 h. In such cases, the composition determined at the matrix–precipitate interface was chosen as the equilibrium value.

The experimental results are presented in the form of the partial isothermal section shown in Fig. 2. The section is characterized by five three-phase fields where the phase R2:17, based on Sm_2Co_{17}, is in equilibrium successively with Co, Zr_6Co_{23}, the phases

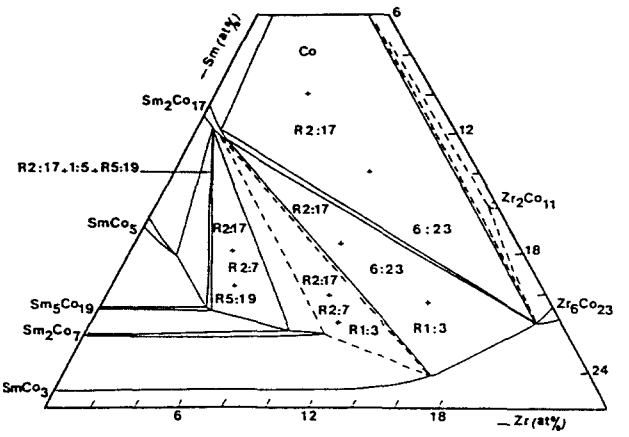

Fig. 2. Partial isothermal section of the system Sm–Co–Zr at 850°C.

$n + 1{:}5n - 1$ based on $Sm_{n+1}Co_{5n-1}$, and $SmCo_5$. The compositions and the lattice parameters of the limiting phases of the tie-triangles are reported in Table 1.

3.1.1. Comparison of the phase equilibria at 1150 and 850°C

Some identical features are observed: the very limited Sm solubility in Co and Zr_6Co_{23}, the extended substitution range of Zr for Sm in the phases $n + 1{:}5n - 1$. At 850°C the Zr solubility is about the same as at 1150°C, but the Co content is closer to the stoichiometric ratio $n + 1{:}5n - 1$. The rhombohedral form of the crystal structures described for $Sm_{n+1}Co_{5n-1}$ [9] has been observed. The diffraction peaks are finer and more numerous at 850°C than at 1150°C. The substitution of Zr for Sm produces a slight decrease of the lattice parameters.

Two significant changes are evidenced:

— regions involving an equilibrium between Zr_2Co_{11} and the 1:7 phase are no longer detected;

— the extended ternary single phase 1:7 reduces to a very limited field around $SmCo_5$. The Zr solubility in $SmCo_5$ is about 2 at.%. On the Co-rich side of the as-quenched 1:7 phase, the compound Sm_2Co_{17}, with the rhombohedral structure, forms a narrow existence range along the line corresponding to the substitution of Zr for Co pairs. Owing to kinetic problems already described, the Zr solubility limit in $SmCo_5$ and Sm_2Co_{17} is defined by an uncertainty of 0.5–1 at.%.

The evolution of the phase equilibria from 1150 to 850°C mainly involves the decomposition of the 1:7 phase. Besides the very sluggish growth rates related to this decomposition, very different microstructures are generated, depending on the content of the initial 1:7 phase. Consequently, the investigation of the microstructural features of the decomposed 1:7 phase is used to identify the phase transformation processes.

Table 1
Phase compositions and lattice parameters of the three-phase domains

	1:5	R2:17	R5:19	R2:17	R5:19	R2:7	R2:17	R1:3	6:23	R2:17	6:23	Co
Sm (at.%)	15.8	11	16	11	16	13	10.7	7	20.3	10.6	20.5	0.8
Zr (at.%)	2	0.6	5	0.6	5	9.5	1.7	17	1.2	1.2	1.1	0.1
a (nm)	0.498	0.84	0.498	0.84	0.498	0.497	0.84	0.497	1.154	0.84	1.155	—
c (nm)	0.3987	1.22	4.788	1.22	4.788	3.579	1.22	2.398		1.22	—	—

3.2. Mechanisms involved in the decomposition of the 1:7 phase

3.2.1. Transformations predicted from the phase equilibria

By comparing the equilibria at 1150 (initial state) and 850°C (final state), the decomposition of the 1:7 phase is expected to proceed by two different processes in the composition ranges referred to as I and II in Fig. 3. In I, the depletion of the supersaturated matrix 1:7 must occur by continuous precipitation of R2:17 and/or 5:19 according to reactions such as 1:7 → 1:5 + R2:17. In II, the reactions correspond to the scheme 1:7 → R2:17 + *Co* + 6:23. They should entail the complete decomposition of 1:7 by a discontinuous process. These predictions assume that the coherent phases formed during the first steps of the 1:7 decomposition are the stable equilibrium phases. This behaviour is not expected for concentrations around Sm11.5, Zr2.5 at.% that correspond to permanent magnet compositions. The transmission electron microscopy (TEM) studies of these materials in the coherent steps [4] showed the nucleation and growth of stable R2:17 cells and of the metastable 1:3 platelets from the 1:7 matrix retained as metastable 1:5 cell boundaries. In the incoherent state [10], 1:5 and 1:3 evolve towards the equilibrium phases 5:19 and 2:7. Then, the microstructure change with the aging time is examined to check the processes predicted along the 1:7 domain.

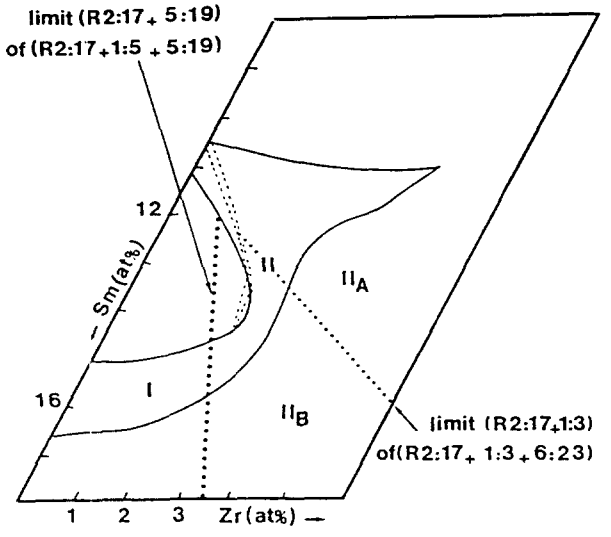

Fig. 3. Composition ranges of the different decomposition processes of 1:7, quenched or cooled from 1150°C; I: continuous precipitation, predicted and observed for the depletion 1:7(+5:19) → 1:5 + R2:17(+5:19); II: discontinuous precipitation (DP) predicted for the reactions 1:7 → R2:17 + *x*; II_A: DP observed for 1:7 → R2:17 + Co + 6:23 and 1:7 → R2:17 + 6:23 + 1:3; II_B: DP not observed for 1:7 → R2:17 + 5:19 + 2:7 and 1:7 → R2:17 + 2:7 + 1:3.

3.2.2. Transformations analysed from the microstructure evolution

Domain I. The behaviour is well represented by the single phase with composition Sm14.7, Zr1.5 at.% in the as-quenched state of 1:7. After aging at 850°C, the microstructures (Figs. 4(a) and 4(b)) reveal homogeneous precipitation of R2:17 plates parallel to the basal plane of the 1:5 matrix and precipitate-free zones (PFZ) along the grain boundaries where R2:17 is coarsened. Increasing aging time leads mainly to growth of the existing precipitates and the increase in Zr and Sm contents of the 1:5 matrix. The microstructural features are consistent with the predicted continuous precipitation. In specimens aged for 160 h, concentration gradients are detected in the 1:5 matrix close to the R2:17 precipitates, the composition of the latter being constant. The concentration profile plotted along the basal plane of 1:5 (Figs. 4(c) and 4(d)) is characteristic of a diffusion mechanism.

The three-phase field, formed by the reaction 1:7 + 5:19 → 1:5 + R2:17 + 5:19, also displays the features of the continuous precipitation of R2:17 in 1:5. The 5:19 phase, the composition of which is about the same at 1150 and 850°C, is not involved in the process. In one of the studied specimens, the amount of R2:17 precipitated after 600 h is small (Fig. 5(a)) and the concentration profile of the depleted matrix (Fig. 5(b)) can be analysed assuming infinite extent conditions. Along the distance x from the interface R2:17–1:5, the measured variation of the Zr content C_x is well represented by the equation:

$$C_x = C_o - (C_o - C_i)\{1 - \mathrm{erf}[x/(4\tilde{D}t)^{1/2}]\}$$

where C_o, C_i are the Zr contents in the saturated matrix and at the interface respectively, $\tilde{D}$ is the diffusion coefficient and t is the aging time.

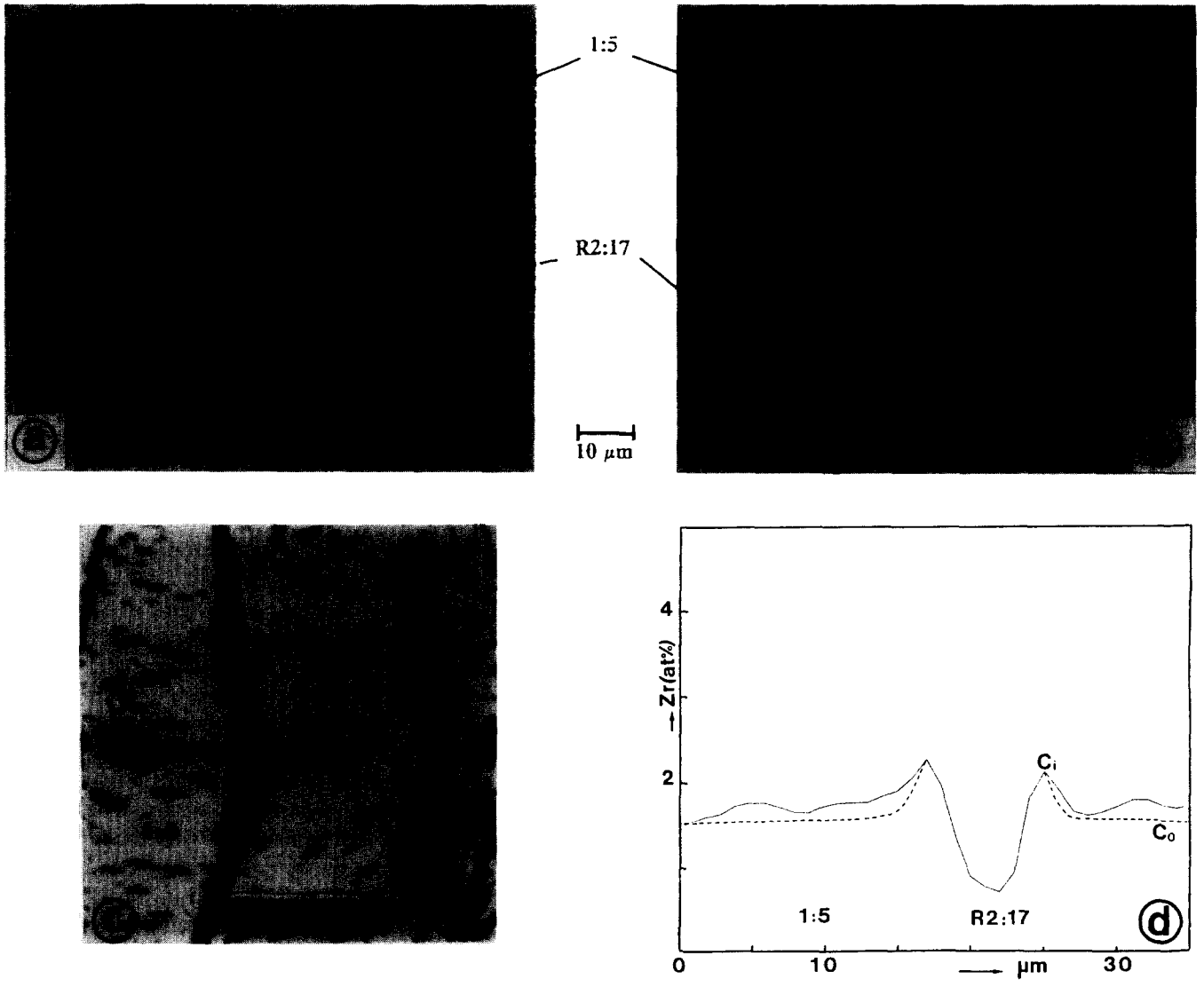

Fig. 4. Alloy with composition $Sm_{14.7}$, $Zr_{1.5}Co_{83.8}$ (at.%) aged at 850°C. Microstructures after (a) 160 h and (b) 600 h; (c) micrograph of the region scanned by EPMA in the specimen aged for 160 h, the arrow indicates the length and the direction of the concentration variation through the sequence 1:5–R2:17–1:5; (d) Zr content profile along the line corresponding to the arrow: ———, measured; – – –, calculated. C_o, C_i are the Zr contents in the saturated matrix and at the interface.

This leads to an evaluated magnitude range of the diffusion coefficient in 1:5 equal to 30×10^{-20} m^2 s^{-1}.

This value also provides a consistent representation of the Zr content variation of the aged Sm14.7, Zr1.5 at.% alloy described in Fig. 4(d).

Domain II. According to their microstructures, the aged samples with various compositions in domain II can be classified in two groups, referred to as II_A and II_B in Fig. 3.

The first group (II_A) corresponds to Co and Zr contents larger than the limit tie-line (R2:17 + 1:3) of the triangle (R2:17 + 1:3 + 6:23). As demonstrated by the aging behaviour of the quenched phase 1:7 with composition Sm10.5, Zr2 at.%, the microstructures are characteristic of discontinuous precipitation. The samples treated 80 to 240 h at 850°C (Fig. 6) show duplex zones, consisting of lamellae parallel to the matrix basal plane, that form regular layers along the grain boundaries. The duplex zone thickness increases with aging time (about 5 μm at 80 h, 16 μm at 240 h) and completely fills the grains after 720 h. The lamellae spacing, about 2 μm, is too small for a reliable EPMA determination of the lamellae composition. However, the analysis of the coarsened phases along the grain boundaries identifies the phases as R2:17, 6:23 and Co, formed at the expense of the supersaturated matrix 1:7. The latter phase was observed in the grain centre. The consistent results obtained by XRD also revealed

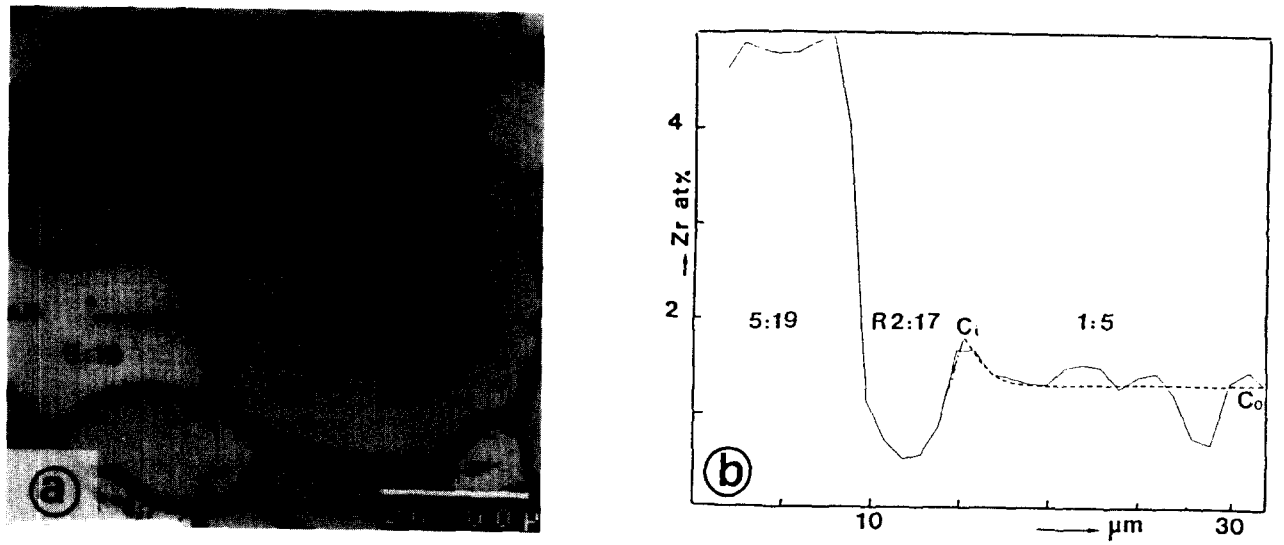

Fig. 5. Specimen in the field (1:5 + 5:19 + R2:17) aged 850°C, 600 h. (a) Microstructure of the region scanned by EPMA, the arrow shows the length and the direction of the concentration variation through the sequence 5:19–R2:17–1:5; (b) Zr content profile along the line corresponding to the arrow: ———, measured; – – –, calculated.

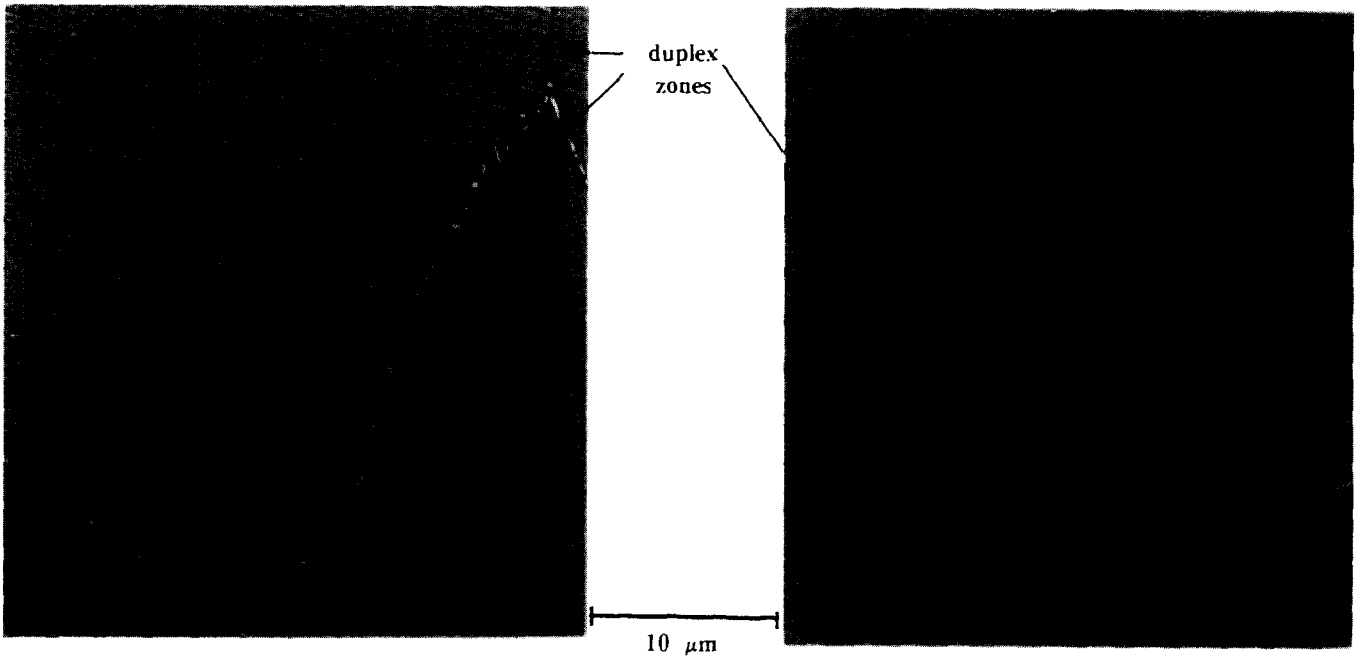

Fig. 6. Microstructure of the alloy with composition $Sm_{10.5}Zr_2Co_{87.5}$ (at.%) aged at 850°C: (a) 80 h; (b) 240 h.

an increase of the R2:17 superstructure peaks with aging time, indicating the gradual decomposition of the disordered 1:7 matrix. This leads to a description of the duplex zones as the alternate stacking of 'large' R2:17 lamellae and fine (6:23 + Co) films. The clear-cut analysis of the concentration profile (Fig. 7) in the specimen aged for 240 h is difficult because the duplex zone composition corresponds to a mixture of the R2:17 and 6:23 lamellae. However, the typical curve expected along the sequence R2:17 lamellae–supersaturated 1:7 matrix, for a transformation rate limited by diffusion [11], is consistent with the Zr content variation recorded in the experimental profile.

The group II_B is found between the tie-triangles (R2:17 + 1:3 + 6:23) and (R2:17 + 1:5 + 5:19). After aging, the as-quenched 1:7 phase located in this concentration field displays a microstructure reminiscent of the typical cell network of 2:17 permanent magnets. An example is given by the micrographs (Figs. 8(a) and 8(b)) of the alloy with Sm11, Zr2.5 at.% aged for 80 and 240 h. The phase sizes, that do not exhibit a significant coarsening even after 600 h, are

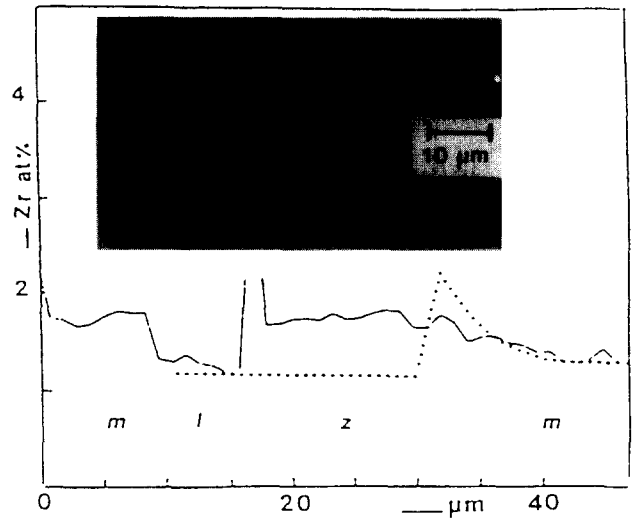

Fig. 7. Zr concentration profile through the sequence twinned matrix 1:7 (m)–R2:17 (l)–duplex zone (z)–twinned matrix 1:7(m): ———, measured; · · · typical [11].

too small for EPMA or SEM investigations. XRD detects R2:17 and an evolution of the initial 1:5 spectrum towards the superstructures $n+1{:}5n-1$ with aging time. This evolution is expected from the results of the phase diagram at 850°C.

Obviously, the equilibrium results were not obtained on such fine structures. They were obtained from specimens with overall compositions in the fields $(1{:}7+n+1{:}5n-1)$ at 1150°C. In this case (Fig. 9) the phases $n+1{:}5n-1$ formed at 1150°C are large and easy to analyse. Their small composition change from 1150 to 850°C occurs by continuous precipitation of R2:17. As for R2:17 produced by 1:7 decomposition, this is coarse enough for analysis when located along the grain or interphase boundaries. Inside the previous 1:7 grains, a microstructure such as described

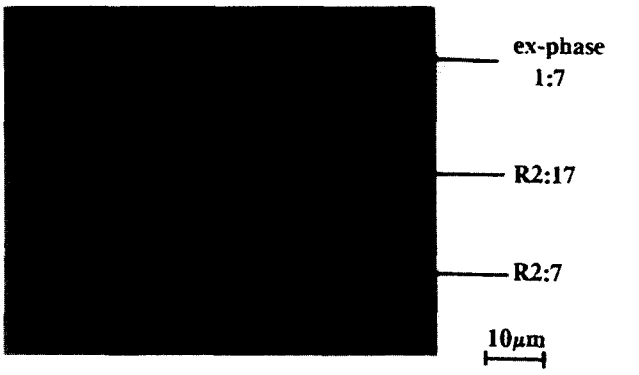

Fig. 9. Microstructure of the alloy with composition $Sm_{12.3}Zr_{2.8}Co_{84.9}$ (at.%) aged 850°C, 600 h.

in Fig. 8 is present: this does not point to a discontinuous process. This genesis could be deduced from the TEM results on the quinary alloys $Sm_{11.5}(Co_{58.3}Fe_{22.5}Cu_{5.3})Zr_{2.4}$ [4] and $Sm_{12.2}(Co_{60.6}Fe_{19.3}Cu_{5.3})Zr_{2.6}$ [10] with compositions similar to the studied alloys, as far as a similar behaviour is found for Co, Fe and Cu. This corresponds to two steps: (1) continuous nucleation and growth of R2:17 cells and subsequently of 1:3 platelets; this proceeds in the metastable coherent field and is controlled by diffusion; (2) very sluggish transformation towards the incoherent stable state R2:17 + 5:19 + 2:7 (or 2:7 + 1:3) by a mechanism not previously studied.

4. Conclusion

The purpose of the present study was to determine the phase equilibria of the system Sm–Co–Zr at 850°C, but the main results concern the decomposition

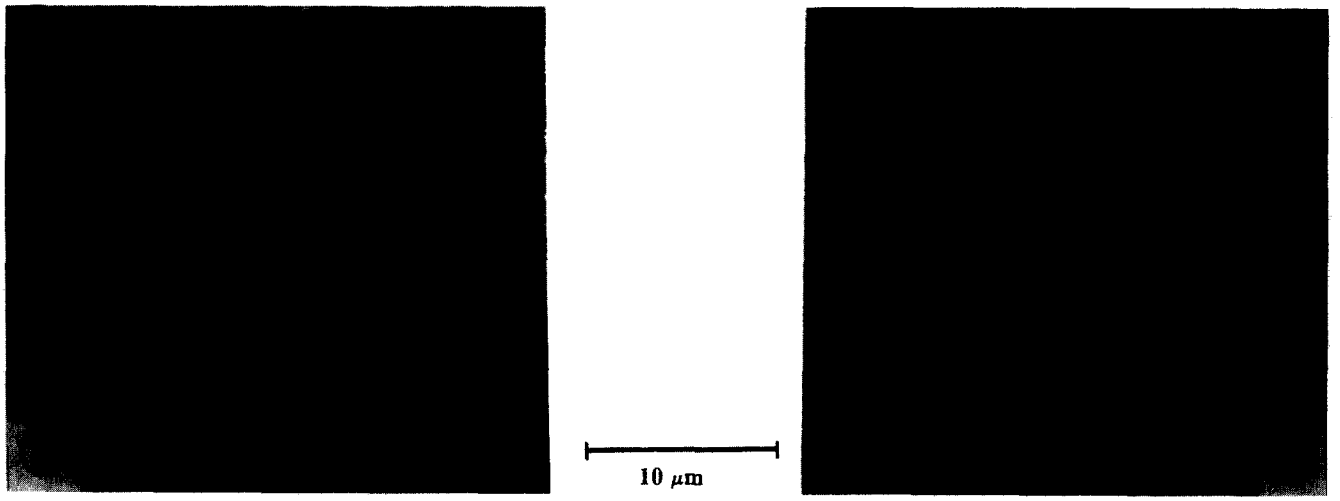

Fig. 8. Microstructure of the alloy with composition $Sm_{11}Zr_{2.5}Co_{86.5}$ (at.%) aged at 850°C: (a) 80 h; (b) 240 h.

processes of the supersaturated 1:7 phase leading to the equilibrium state.

In agreement with the provisions based on the attainment of equilibrium from 1150 to 850°C, the microstructures show that:

— in region I, corresponding to the reactions 1:7 → 1:5 + R2:17 and 1:7 + 5:19 → 1:5 + R2:17 + 5:19, the 1:7 depletion occurs by continuous precipitation;

— in region II_A, defined by the reactions 1:7 → (R2:17 + *Co* + 6:23) and 1:7 → (*R*2:17 + 6:23 + 1:3), the 1:7 decomposition proceeds by discontinuous precipitation.

In regions I and II_A, the growth rates are controlled by diffusion.

In the intermediate region II_B, the microstructures do not support the discontinuous mechanism expected for the reactions 1:7 → R2:17 + 5:19 + 2:7 and 1:7 → R2:17 + 2:7 + 1:3. They suggest the genesis of the coherent metastable state 1:5 + R2:17 + 1:3 by continuous nucleation and growth. The further transformations leading to the incoherent stable phases have yet to be studied.

All the processes involving the R2:17 formation evidence its instant nucleation as detectable by XRD, followed by very sluggish growth. This explains why no significant difference is found between the specimens aged after quenching (Q) or after slow cooling (C). This behaviour has already been demonstrated for R2:17 and 1:3 in magnet materials, and related to a slow diffusion rate. The $\tilde{D}_{1:5}$ value presently determined is higher than estimated from the R2:17 cell growth in the magnets [4]. Concerning $\tilde{D}_{1:5}$, this is calculated from experimental results acquired in conditions close to the assumptions of the theoretical approach (no diffusion in the R2:17 precipitates, infinite extent). Its value should represent correctly the diffusion behaviour in domain I. Concerning $\tilde{D}$, this was estimated for the composition of the magnets equivalent to the value in domain II_A. In this region, R2:17 is generated in large amounts by 1:7 depletion and has a significant existence range, at least in the coherent state. The precise analysis of the growth rate should take into account the diffusional fluxes in R2:17 and 1:5 and finite diffusion lengths. However, the smaller magnitude for $\tilde{D}$ than for $\tilde{D}_{1:5}$ reflects that the growth rate is slower in I than in II, which is experimentally observed. In the future, a more precise determination of the diffusion characteristics in domain II will be carried out.

Acknowledgements

We are grateful to the Direction de la Recherche et de la Technologie de la Délégation Générale pour l'Armement du Ministère de la Défense for their financial support (contract 94: 2612 A/DRET).

References

[1] Y. Morita, T. Umeda and Y. Kimura, *J. Jpn. Inst. Met., 50* (1986) 235.
[2] Y. Morita, T. Umeda and Y. Kimura, *IEEE Trans. Magn. 23* (1987) 2702.
[3] T.S. Chin, W.C. Chang, R.T. Chang, M.P. Hung and H.T. Lee, *IEEE Trans. Magn., 25* (1989) 3782.
[4] C. Maury, L. Rabenberg and C.H. Allibert, *Phys. Status Solidi A, 140* (1993) 57.
[5] T. Nishio, Y. Fukui and Y. Iwama, *J. Jpn. Inst. Met., 52* (1988) 502.
[6] S. Derkaoui, N. Valignat and C.H. Allibert, *J. Alloys Comp.*, in press.
[7] W.Q. Ge, C.H. Wu and Y.C. Chuang, *Z. Metallkd., 84* (1993) 165.
[8] W.H. Pechin, D.E. Williams and W.L. Larsen, *Trans. ASM, 57* (1964) 464.
[9] E. Parthé and R. Lemaire, *Acta Crystallogr. B, 31* (1975) 1879.
[10] F. Delannay, S. Derkaoui and C.H. Allibert, *J. Less-Common Met., 134* (1987) 249.
[11] J.W. Christian, in R.W. Cahn (ed)., *Physical Metallurgy*, North-Holland, Amsterdam, 1970, Chapter 10, p. 512.